The Force Generation Mechanism of Lifting Surfaces with Flow Separation

I.M. Viola[a,*], Abel Arredondo-Galeana[b] and Gabriele Pisetta[a]

[a] Institute for Energy Systems, School of Engineering, University of Edinburgh, Edinburgh, EH10 5HD, UK
[b] Formerly: Institute for Energy Systems, School of Engineering, University of Edinburgh, Edinburgh, EH10 5HD, UK.
Currently: Department of Naval Architecture, Ocean & Marine Engineering, University of Strathclyde, Glasgow, G4 0LZ, UK

ARTICLE INFO

Keywords:
Lifting surface
Hydrofoil/Blade Hydrodynamics
Wing/Sail Aerodynamics
Leading-edge separation
Impulse theory
Lifting-line theory

ABSTRACT

Fins, wings, blades and sails can generate lift and drag in both attached and separated flow conditions. However, the common understanding of the *lift* generation mechanism holds only for attached flow conditions. In fact, when massive flow separation occurs, the underlying assumptions of thin airfoil theory and lifting line theory are violated and the concept of bound circulation cannot be applied. Therefore, there is a need to develop an intuitive understanding of the force generation mechanism that does not rely on these assumptions. This paper aims to address this issue by proposing a paradigm based on established concepts in theoretical fluid mechanics, and impulse theory in particular. The force generation can be intuitively associated with the vorticity field, which can be gathered with computational fluid dynamics or particle image velocimetry. This paradigm reconciles key known results about wing aerodynamics, and provides designers of lifting surfaces a measurable objective to optimise the shape in separated flow conditions. It will hopefully underpin both a deeper understanding of how lift and drag are generated, and the development of low order models in different fields of application.

1. Introduction

1.1. The Origin of Lift

The origin of lift is one of the most fundamental questions in fluid dynamics and one of the most difficult to explain in simple terms. Despite its critical significance, there is not as yet a satisfactory explanation on the origin of lift for the layperson (Regis, 2020). The most common understanding is based on the concept of circulation that was developed independently in the early 1900s by Lanchester (1907) in the UK, Kutta (1902) in Germany and Joukowsky (1906), sometimes Jukowsky or Zhukovsky, in Russia.

In summary, a solid body immersed in a moving fluid results necessarily in fluid rotation (Ω), whose measure is the vorticity ($\omega = 2\Omega$); and the integral of the vorticity over a surface is the circulation (Γ). A solid body within a moving fluid must be immersed in a layer of vorticity to ensure a non-slip velocity at the interface. If the overall integral of vorticity is not null, then there is bound circulation (Γ_b) around the body.

The simplest model of a two-dimensional lifting surface, i.e. a foil, is a point vortex with circulation equal to the integral of all of the vorticity in its boundary layer. The lift can be easily computed by considering a convenient solid surface of arbitrarily radius a around the vortex. For example, a solid surface can be included in a complex potential through a doublet of arbitrary strength, resulting in a closed streamline representing a solid cylinder. Then one can compute the velocity on the cylinder surface as the vectorial sum of the free stream velocity and the vortex-induced velocity, and use the Bernoulli equation to compute the pressure distribution around the cylinder. The pressure integral in the lift direction on the cylinder surface is the lift per unit depth. The result is $L = -\rho U \Gamma_b$, which is the Kutta-Joukowsky theorem. This theorem shows that the lift (per unit depth) depends only on fluid density ρ, the free stream velocity U and the bound circulation Γ_b. An equivalent formulation was derived by Filon (1926) for the drag (per unit depth): $D = \rho U Q_\psi$, where Q_ψ is the net flow rate into the wake of the vector potential derived by Helmholtz decomposition. Unfortunately, however, Q_ψ cannot be directly measured (Liu et al., 2015).

The force production mechanism is explained in terms of bound circulation in, for example, virtually all of the sail aerodynamics books (e.g. Whidden and Levitt, 1990; Larsson and Eliasson, 1995; A. R. Claughton et al., 1998; Fossati, 2009; van Oossanen, 2018, etc.). As discussed in the following, this model is fairly accurate for lifting surfaces where the vorticity is confined within the boundary layer. Moreover, it allows the interaction between the two lifting surfaces to be explained intuitively, and it explains why the Venturi effect does not generally apply in unbounded flows. For example, the Venturi effect has often been incorrectly considered to explain the interaction between two sails (Gentry, 1971, 1973). On the other hand, when flow separation occurs, the concept of bound circulation is not very helpful and we lack an intuitive understanding of the force generation mechanism.

1.2. Lifting Surfaces with a Sharp Leading Edge

* This work received funds from the UK Engineering and Physical Sciences Research Council (EPSRC) via the EPSRC Centre for Marine Energy Research (EP/P008682/1), the EPSRC Centre for Advanced Materials for Renewable Energy Generation (EP/P007805/1), the EPSRC Centre for Doctoral Training in Wind and Marine Energy Systems (EP/L016680/1) as well as research grant EP/R511687/1.

*Corresponding author
i.m.viola@ed.ac.uk (I.M. Viola)
www.voilab.eng.ed.ac.uk (I.M. Viola)
ORCID(s): 0000-0002-3831-842 (I.M. Viola)

This is a peer-reviewed, accepted author manuscript of the following article: Viola, I. M., Arredondo-Galeana, A., & Pisetta, G. (2021). The force generation mechanism of lifting surfaces with flow separation. Ocean Engineering, 239, [109749]. https://doi.org/10.1016/j.oceaneng.2021.109749

Flow separation occurs at the leading edge of lifting surfaces such as fins, wings, blades and sails, when the radius of curvature of the leading edge is small compared to the chord length. For such geometries, there is only one angle of attack, namely the ideal angle of attack, where the onset flow is tangent to the leading edge and an attached boundary layer develops on both sides of the solid surface. At any other other angle of attack, the flow separates on one of the two sides of the surface. For an angle of attack higher than the ideal one, vorticity is shed downstream towards the suction side of the surface and rolls up into vortices, which might then roll along the solid surface or be shed away (Owen and Klanfer, 1955; Gault, 1957; Chang, 1970; Arena and Mueller, 1980; Carter and Vatsa, 1984; Newman and Tse, 1992; Crompton and Barrett, 2000; Stevenson et al., 2016a,b). The rolling of these vortices results, in a time averaged sense, in flow reattachment and in a recirculation region near the leading edge that is known as leading-edge separation bubble. This occurs, for example, at the leading edge of headsails on sailing yachts (Milgram, 1998; Viola and Flay, 2011b; Viola et al., 2013b; Souppez et al., 2019a,b).

On low-aspect-ratio wings, because the flow is strongly three-dimensional, the circulation shed by the shear layer might roll up into a leading-edge vortex that remains steadily attached to the leading edge (Viola and Flay, 2011a,c; Viola et al., 2013a, 2014; Bot et al., 2014; Richards and Viola, 2015; Deparday et al., 2018; Arredondo-Galeana and Viola, 2018). The condition leading to the stability of leading-edge vortices on low-aspect-ratio wings is the objective of several recent studies including Maxworthy (2007); Widmann and Tropea (2015); Muir and Arredondo-galeana (2017); Akkala and Buchholz (2017); Marzanek and Rival (2019); and Eldredge and Jones (2019).

To understand the underlying force generation mechanism, it is useful to simplify the geometry to the essential features that explain the key observed phenomena. In particular, lifting surfaces with leading-edge separation can be described as flat plates at incidence (Roshko, 1954, 1955; Sarpkaya, 1975; Kiya and Arie, 1977), and the effect of camber, aspect ratio, swept and twist can be considered separately. For example, the sharp leading edge of the plate and of the sail leads to similar separated flow fields at those angles of attack where a foil with a curved leading edge would, instead, experience an attached boundary layer. Hence, the flow around a plate is adopted in this paper to elaborate the proposed paradigm of lifting surfaces with leading-edge separation.

For a list of flat plate studies, interested readers can find a useful table in Afgan et al. (2013). The effect of curvature (Dugan and Cisotti, 1970; Sunada et al., 1997, 2002; Okamoto and Azuma, 2005) can be considered as an increase of the effective angle of attack. Studies on highly-cambered circular arcs (Bot, 2019; Nava et al., 2016; Collie et al., 2009; Cyr and Estelle, 1992; Bot et al., 2016; Bot, 2019) allow one to isolate the underlying differences between low and highly cambered plates. The favourable pressure gradient upstream of the maximum chamber on a cambered plate promotes reattachment and the establishment of an attached boundary layer, which is unlikely to occur on a flat plate. On the other hand, on the rear of a cambered plate, the adverse pressure gradient promotes trailing edge separation. For example, recent work (Flay et al., 2017; Bot, 2019; Souppez et al., 2021) has focused on the leading-edge separation bubble of circular arcs and on how it affects trailing edge separation, which is a phenomenon that occurs on cambered plates and not on flat plates.

The main effect of the finite aspect ratio and of the sweep angle is to promote spanwise convection of vorticity, which, for example, can enable a stable leading-edge vortex. The effect of the aspect ratio on the aerodynamics of flat plates was comprehensively reviewed by Taira and Colonius (2009), Lee et al. (2012), and Devoria and Mohseni (2017). Similarly, for the effect of sweep angle, consider the literature survey of Huang et al. (2015).

Finally, it is instructive to note that the effect of twist is the same as that of a shear in the onset flow, and that the twist does not change the slope of the lift curve versus the angle of attack (Phillips, 2004). Hence, two lifting surfaces with the same shape but different twist, would result in the same lift versus angle of attack curve.

1.3. Aim and Organisation of the Paper

The aim of this paper is to propose a paradigm for the force production of lifting surfaces that is applicable both in attached and separated flow conditions. This is based on well understood fluid mechanics principles, which, however, are not commonly applied in naval architecture and sail aerodynamics. This is the vorticity-moment theory, or impulse theory, that describes the forces as the time derivative of the fluid impulse, which can be computed from the vortex flow in the whole flow field. The advantage of this approach is that it allows an intuitive rationale for how both lift and drag are generated in both attached and separated flow conditions, both in steady and unsteady conditions. More specifically, it reveals the force contribution associated with any element of vorticity in the fluid. For example, it shows how the vorticity in different regions of separated flow is associated with the forces generation. Hence, it allows the force differences between two flow conditions with separated flow to be interpreted. This can guide designers to identify the optimum shape and to identify desirable and undesirable flow features in the fluid.

The vorticity-based approach is equivalent to the common pressure-friction approach. However, while knowledge of the surface pressures on the solid surface allow the areas that most contribute to a force direction to be identified (e.g. Viola et al., 2013b), the pressure in the flow field does not provide any direct information of its effect on the forces experienced by the body. For example, a vortex on the suction side of a lifting surface is typically assumed to decrease the surface pressure and thus to lead to lift enhancement. However, the presence of a local pressure minimum in the fluid region does not necessarily result in a low pressure on the body surface itself. In fact, we show in §2 that the force contribution associated with such a vortex depends on the sign of its circulation and on its velocity. Some vortices in the separated flow region are associated with a positive lift contribution and drag reduction, while others are associated with lift reduction and a drag increase.

The impulse theory is an equivalent formulation to the Navier-Stokes equations and, therefore, could be written in a formulation appropriate for numerical modelling, such as in the discrete vortex methods (Katz, 1981). However, in this paper we do not consider these numerical methods and we focus on how this theory can be used to interpret the observed flow fields. Interpreting the force generation mechanism can, in turn, underpin low-order models to predict the forces (Babinsky et al., 2016; Stevens et al., 2016; Corkery and Babinsky, 2018; Chowdhury and Ringuette, 2019). Hence, whilst the proposed paradigm is not a predictive model per se, it is envisaged that it will underpin low order models for lifting surfaces experiencing separated flow in different applications.

The rest of the paper is organised as follows. In §2 we introduce the impulse theory. Then, we show how it provides a physical interpretation of the force generation mechanism in two-dimensional (2D) flow (§3) and three-dimensional (3D) flow (§4). In §5 we consider how the force generation mechanism is affected by other solid bodies in the fluid, and in §6 by free vorticity in the fluid. Finally, the results and their significance are summarised in §8.

2. Impulse Theory

From Newton's second law, we readily find that the force $\boldsymbol{F}$ on a body is given by the time derivative of the impulse. For a volume of fluid V_f with constant density ρ, whose external boundaries approach infinity,

$$\boldsymbol{F} = -\int_{V_f} \rho \frac{\mathrm{d}\boldsymbol{u}}{\mathrm{d}t}\,\mathrm{d}V = -\rho \frac{\mathrm{d}}{\mathrm{d}t}\int_{V_f} \boldsymbol{u}\,\mathrm{d}V = -\rho\frac{\mathrm{d}\boldsymbol{I}}{\mathrm{d}t}, \quad (1)$$

where ρ is the fluid density, t is time, $\boldsymbol{u}$ is the velocity vector and

$$\boldsymbol{I} = \int_{V_f} \boldsymbol{u}\,\mathrm{d}V \quad (2)$$

is the impulse. Bold symbols denote vectors.

Wu (1981) and Lighthill (1986) showed that the impulse is given by

$$\boldsymbol{I} = \frac{1}{n_d - 1}\left(\int_{V_f} \boldsymbol{x}\times\boldsymbol{\omega}\,\mathrm{d}V + \int_{S_b} \boldsymbol{x}\times(\boldsymbol{n}\times\boldsymbol{u})\,\mathrm{d}S\right), \quad (3)$$

where $n_d = 2$ and 3 in two and three dimensions, respectively, $\boldsymbol{x} = (x, y, z)$ is the coordinate vector, $\boldsymbol{\omega}$ is the vorticity vector, S_b is the solid boundary within V_f (e.g. the surface of a wing), and $\boldsymbol{n}$ is the outward unit normal of S_b. A complete derivation and discussion is available in, for instance, Eldredge (2019) (p. 190).

The second term of eq. 3 vanishes in a reference system fixed with the body. This, in fact, is an unsteady body force equal to the difference between the forces as observed from the reference system $O(x, y, z)$ and those observed from a reference system fixed with the body. It is proportional to the product of the fluid density and the body volume (Koumoutsakos and Leonard, 1995; Leonard and Roshko, 2001) and thus its effect is negligible for slender bodies with small volume to surface area ratio (Rival and van Oudheusden, 2017). For bodies whose weight is supported by the fluid dynamics forces such as a flying body, Lentink (2018) noted that this unsteady body force is also negligible for small fluid to body density ratio.

Equation 3 was derived independently by Wu (1981) and Lighthill (1986) unaware of each other's work. They defined it as the momentum theorem (based on vorticity moments) and impulse theory, respectively. It allows the computation of the forces on a body from the knowledge of the vorticity in the flow field. Key physical constrains that these models should satisfy are the Kutta condition and Kelvin's theorem. The Kutta condition states that the trailing edge of a slender body must be a stagnation point. Consequently, the stagnation streamline is tangent to the bisector of the trailing edge in steady flow, and tangent to one of the two sides of the trailing edge in unsteady flows (Basu and Hancock, 1978; Katz, 1981). In turn, this condition sets the amount of vorticity that is shed at the trailing edge by the solid body into the wake. Kelvin's theorem states that the circulation computed along a closed contour that moves with the fluid, remains constant over time if the fluid is inviscid or irrotational *at* the contour. For example, consider a foil starting from rest in uniform flow, such that the vorticity vanishes at infinity. A closed contour including the foil and approaching infinity would lie in irrotational flow. Thus Kelvin's theorem states that the circulation must be zero, as it was before the foil started moving. Hence, the positive and negative vorticity must balance and the net vorticity in the fluid must remain zero over time.

3. Two-dimensional Flow

Consider a two-dimensional space, a rigid body and negligible unsteady body forces. This allows the derivation to be simplified without loss of generality. From equations 1-3, we find that the force per unit depth is

$$\boldsymbol{F} = -\rho\frac{\mathrm{d}}{\mathrm{d}t}\int_{V_f} \boldsymbol{x}\times\boldsymbol{\omega_z}\,\mathrm{d}S. \quad (4)$$

Now consider the vorticity to be concentrated in pairs of counter-rotating vortices with circulations $-\boldsymbol{\Gamma}$ and $\boldsymbol{\Gamma}$. Then the force $\boldsymbol{F}$ in the direction orthogonal to the segment $\boldsymbol{d}$ is (Kim and Gharib, 2011; Babinsky et al., 2016):

$$\boldsymbol{F} = \rho\Sigma_i(\dot{\boldsymbol{\Gamma}}_i \times \boldsymbol{d}_i + \boldsymbol{\Gamma}_i \times \dot{\boldsymbol{d}}_i), \quad (5)$$

where the dot denotes time derivative, and the force is positive in the direction from the centroid of the vortex with negative circulation to that of positive circulation. This is, in fact, the time derivative of the impulse of vortex pairs, whose impulse was found by Lamb (1932) to be $\rho\Gamma d$, with

$\Gamma \equiv |\mathbf{\Gamma}|$. The rate of change of the circulation $\dot{\mathbf{\Gamma}}$ should be understood as the production rate of new vortex pairs, viz. vortex pairs with constant circulation $\mathbf{\Gamma}$ are formed with a period $\delta t = \Gamma/\dot{\Gamma}$.

For a single vortex pair whose centroids are located at coordinates (x_1, y_1) and (x_2, y_2) as in Fig. 1, eq. 5 shows that the lift (L) and drag (D) are

$$L = \rho \left((x_2 - x_1)\dot{\Gamma}_2 + (\dot{x}_2 - \dot{x}_1)\Gamma_2 \right), \tag{6}$$

$$D = -\rho \left((y_2 - y_1)\dot{\Gamma}_2 + (\dot{y}_2 - \dot{y}_1)\Gamma_2 \right). \tag{7}$$

This formulation is independent of the reference system. The subscript of the circulation and of its rate of change shows which coordinates of the vortex must be selected from the two counter-rotating vortices. In the rest of the paper we consider a reference system with the x-axis along the free stream velocity U and positive anticlockwise angles (Fig. 1).

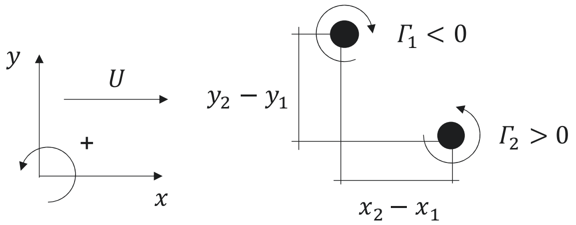

Figure 1: Coordinate system and vortex pair.

3.1. 2D Plate at Low Incidence

Consider a flat plate with chord c at a small angle of attack α, starting from rest and reaching a steady velocity U_b. In a reference system fixed with the plate, the foil is stationary and the fluid flows with velocity $U = -U_b$, as in Fig. 2. The circulation is concentrated near the foil and in the region where the foil was initially at rest, while the net circulation in the wake must vanish in steady conditions. The wake is made of vortex pairs continuously being generated on the two sides of the plate. The distance across which the vorticity is generated is roughly the plate thickness, which is small for a thin plate, thus $\boldsymbol{d} = (x_2 - x_1, y_2 - y_1) \approx (0, 0)$. Also, $\boldsymbol{d}$ remains almost constant, whilst the vortex pairs convect along the plate and then are shed into the wake, thus $\dot{\boldsymbol{d}} \approx (0, 0)$. Consequently, these vortex pairs contribute to neither lift nor drag.

However, in the boundary layer there is a non-zero net circulation. The integral of the vorticity Γ_b around the plate is the bound circulation, while the integral of the vorticity around the region where the plate was initially at rest is the starting circulation $-\Gamma_b$. The bound and starting vortices each have constant circulation and their distance increases at the rate $\dot{\boldsymbol{d}} = (U, 0)$, whilst there is no production of further vortex pairs ($\dot{\Gamma}_b = 0$). Substituting the bound circulation into the impulse theory formulations, eqs. 6 and 7, gives the Kutta-Joukowsky lift theorem and d'Alembert's paradox, respectively:

$$L = -\rho U \Gamma_b \tag{8}$$

$$D \approx 0. \tag{9}$$

This interpretation of the Kutta-Joukowsky lift theorem (eq. 8) reveals that the bound circulation is circulation that moves with velocity U, irrespectively of its nearness to the plate. In other words, all the vorticity in the flow field that moves with velocity U contributes to the bound circulation. This is also in agreement with the concept of trapped vortex studies by Saffman and Sheffield (1977) and successively Huang and Chow (1986). A practical consequence of this result is that the lift can be estimated with eq. 8 by taking the bound circulation as the integral of all of the vorticity in a time averaged flow field. This approach was adopted, for instance, by Devoria and Mohseni (2017), who considered various aspect ratio plates at various incidences. Because in steady conditions the net vorticity flux into the wake must vanish, the integral can be taken over a finite volume around the plate. For example, Lee et al. (2012) investigated flat plates with aspect ratios between one and three, at both low and high angles of attack, which are conditions relevant to yacht sails. They found that the forces computed by integrating the vorticity in the flow field do not vary when the integral is performed over a domain that extends beyond two or three chord lengths downstream of the plate.

For completeness, it is useful to recall that the bound circulation can be computed by considering the plate as a lumped-vortex element; see, for instance, Katz and Plotkin (2001). A vortex with circulation Γ_b is placed at the centre of pressure, which is at the 1/4 chord point of the foil. For a single vortex, the non-penetration condition must be satisfied at only one point, known as the *collocation point*, which can be found to be $c/2$ aft of the vortex (Katz and Plotkin, 2001). At the collocation point, the velocity induced by the vortex is equal in magnitude and opposite in sign to the free stream velocity component normal to the chord, i.e.

$$\frac{\Gamma_b}{2\pi c/2} = -U \sin\alpha. \tag{10}$$

Rearranging, gives the bound circulation as

$$\Gamma_b = -\pi U c \sin\alpha. \tag{11}$$

Substituting the bound circulation from eq. 11 into eq. 8 gives

$$L = \rho U^2 c\, \pi \sin\alpha, \tag{12}$$

and in non-dimensional form

$$C_L = 2\pi \sin\alpha. \tag{13}$$

These results are in agreement with experiments for $\alpha \lesssim 10°$ (Hoerner and Borst, 1975). For example, Fig. 3 and 4 show

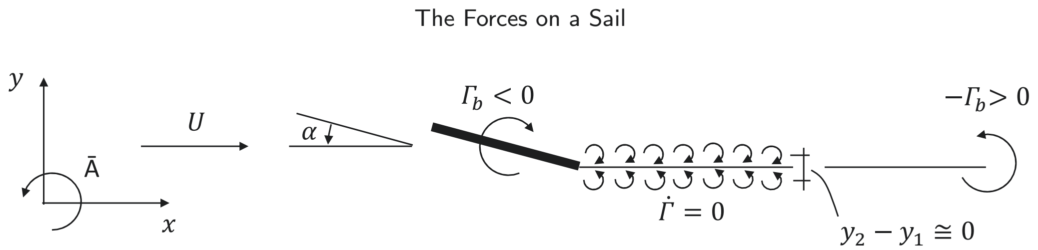

Figure 2: 2D plate at low incidence.

the comparison with the lift and drag coefficients measured by Fage and Johansen (1927) and by the Engineering Science Data Unit (ESDU, 1970). The experiments of Fage and Johansen (1927) were performed at a Reynolds number (Re) of 153k and those of the ESDU at $Re = 54k$.

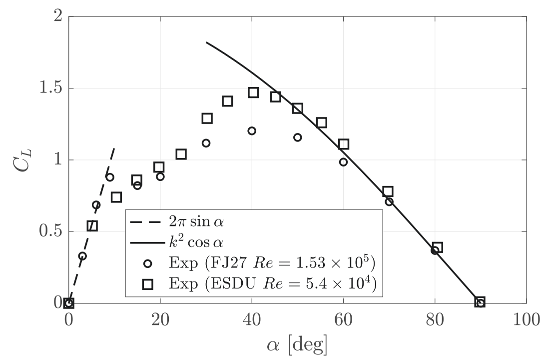

Figure 3: Lift coefficient of a 2D plate versus the angles of attack measured by Fage and Johansen (1927) (FJ27) and (ESDU, 1970) (ESDU), and predictions with eq. 13 ($2\pi \sin\alpha$), and eq. 18 ($k^2 \cos\alpha$).

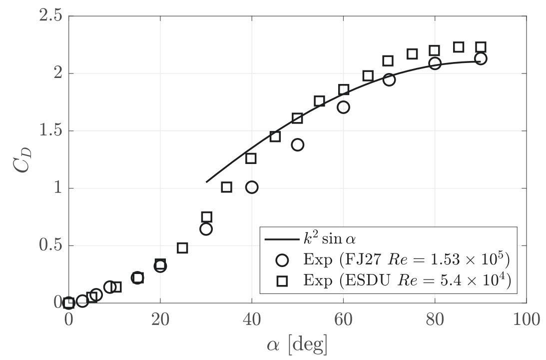

Figure 4: Drag coefficient of a 2D plate versus the angles of attack measured by Fage and Johansen (1927) (FJ27) and (ESDU, 1970) (ESDU), and predictions with eq. 18 ($k^2 \sin\alpha$).

3.2. 2D Plate at High Incidence

Now consider a flat plate at an angle of attack of approximately $\pi/2$ as in Fig. 5. This flow condition was initially investigated as a potential flow with concentrated vorticity by von Helmholtz (1868), who developed the free-streamline theory, and then was further developed by von Kirchhoff (1868) and Lord Rayleigh (1876). Vorticity is shed downstream through two shear layers of opposite sign and equal magnitude at the two edges of the plate.

An estimate of the production of vorticity can be derived from the integral of the flux of vorticity across the shear layers (Fage and Johansen, 1928). Consider a reference system $O'(x', y')$ with x' aligned with a shear layer of thickness δ_{SL}, with streamwise velocity u' ranging from 0 to U_{SL} (Fig. 5). The vorticity production is

$$|\dot{\Gamma}| = -\int_0^{\delta_{\mathrm{SL}}} \omega u' \,\mathrm{d}y' = \int_0^{\delta_{\mathrm{SL}}} \frac{\partial u'}{\partial y'} u' \,\mathrm{d}y' \tag{14}$$

$$= \int_0^{U_{\mathrm{SL}}} u' \,\mathrm{d}u' = \frac{1}{2} U_{\mathrm{SL}}^2, \tag{15}$$

where the boundary layer approximation $\omega = -\partial u'/\partial y'$ is used in the second equality of eq. 14. A similar result was found to be accurate also in unsteady flow conditions (Kiya and Arie, 1977; Basu and Hancock, 1978) for small angles of attack.

Fage and Johansen (1927) noted that, in steady conditions, $U_{SL} = kU$ with $k > 1$. Specifically, they found that k increases from 1.347 at $\alpha = \pi/6$ to 1.49 at $\alpha = \pi/2$ at Reynolds number $Re = 153$k. Roshko (1954) performed similar tests at Re from 3k to 18k, and found k ranging from 1.3 to 1.4 at $\alpha = \pi/2$. The interesting conclusion is that, if leading-edge separation occurs and thus the Kutta condition is established at the leading edge, then there is a force contribution associated with the vorticity production that is $|\dot{\mathbf{\Gamma}}| = \dot{\Gamma} \approx k^2 U^2/2$. Most of this vorticity is generated at the edges, and thus we can assume $\boldsymbol{d} = (c\cos\alpha, -c\sin\alpha)$. When substituted into eqs. 6 and 7, we find that the lift and drag associated with the production of vorticity are, respectively,

$$L = \rho\dot{\Gamma} c \cos\alpha \approx \frac{1}{2}\rho U^2 c\, k^2 \cos\alpha, \tag{16}$$

$$D = \rho\dot{\Gamma} c \sin\alpha \approx \frac{1}{2}\rho U^2 c\, k^2 \sin\alpha, \tag{17}$$

and, in nondimensional form,

$$C_L = k^2 \cos\alpha, \tag{18}$$

$$C_D = k^2 \sin\alpha. \tag{19}$$

The Forces on a Sail

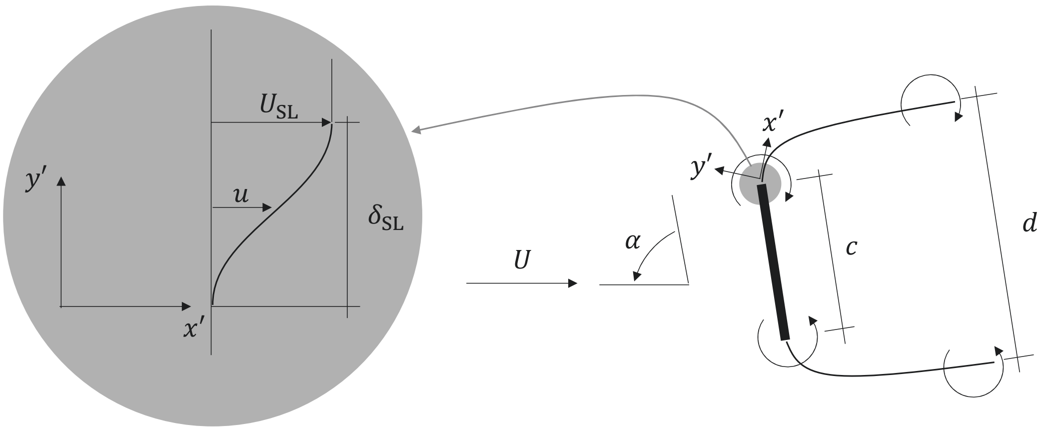

Figure 5: 2D plate at high incidence.

These results could be refined by considering the growth of the wake thickness and vortex annihilation in the wake, see for example the closure of the Kármán solution with free streamline theory by Roshko (1955). While this is beyond the scope of the paper, it is useful to note that the wake thickness d, measured parallel to the chord, does not vary significantly beyond a minimum angle of attack. For example, Fage and Johansen (1927) found that the thickness of the wake measured orthogonal to the stream is $k'c \sin\alpha$, with $k' = 1.475$, for α from $\pi/6$ to $\pi/2$. This implies that the thickness of the wake measured parallel to the plate is constant over this range of incidences.

These results are in good agreement with the forces measured on a flat plate for α between 50° and 90°. Figure 3 and 4 show the lift and drag coefficients predicted with eq. 18 and 19, respectively, where $k = 1.45$ as measured by Fage and Johansen (1928). This value is not universal and different authors have also found different values for similar experiments (e.g. Roshko, 1954). However, the range of variability is relatively small and thus it can be used in a first approximation if direct measurement is not available. The most important result, however, is not the ability to predict the lift and drag with these simple formulations, but rather the physical insights on the force generation mechanism that they provide.

3.3. 2D plate at moderate incidence

At intermediate angles of attack, we do not have a readily available model. However, the following considerations are useful to understand the force generation mechanism. Because the flow is not symmetrical around the streamwise direction, at any instant there is net vorticity near the plate, i.e. $\Gamma_b \neq 0$. However, in separated flow conditions when the vorticity is not confined in a thin boundary layer, it is unclear what should be considered as bound vorticity. For example, if we do not include the vorticity shed in the leading-edge separated shear layer, the bound circulation is positive and it is associated with a negative lift! This counter intuitive result can easily be verified with simulations or experiments by integrating the layer of vorticity enclosing the plate.

In particular, two vortex sheets of equal and opposite sign are shed by the two edges of the plate. The bound circulation ensures that the Kutta condition applies at the two edges. The sum of the plate-normal velocity components due to the vortex sheets, the free stream velocity, and the bound circulation, must vanish at the plate surface. For example, let us assume that the vortex sheets are parallel to the free stream velocity, and that their induced velocity on the opposite side of the plate is negligible. We find that $\Gamma_b = \Gamma_0 \cos\alpha > 0$, where Γ_0 must be positive as demonstrated in the Appendix. The lift is

$$L_b = -\rho U \Gamma_b = -\rho U \Gamma_0 \cos\alpha < 0. \tag{20}$$

However, this is never the only lift component and the total lift is never negative.

A different force generation mechanism is associated with the relative streamwise velocity of leading and trailing edge vorticity. Assuming that the outer velocity is U and the internal velocity is zero, vorticity transported by the shear layer convects with a mean velocity $U/2$. Babinsky et al. (2016) tested a flat plate at incidence and noted that the vorticity shed at the leading edge formed a coherent vortex that convected downstream at about $U/2$, while the vorticity shed at the trailing edge convected with velocity U (Fig. 6). Ōtomo et al. (2021) also found a similar result in the separated flow of large-amplitude pitching foils.

The slower convection of leading-edge vorticity than trailing edge vorticity can occur only for a finite period of time δt. In fact, all of the vorticity in the wake must convect at the same velocity. As an example, assume arbitrarily that a leading-edge vortex (LEV) convects at $U/2$ for a distance $c\cos\alpha$ and thus $\delta t = 2(c/U)\cos\alpha$. In contrast, the associated counter-rotating trailing-edge vortex (TEV), convects with velocity U. Hence, the streamwise stretching of the vortex pairs is associated with a vortex force $\Gamma_{\mathrm{LEV}} = -\dot{\Gamma}\delta t = -2\dot{\Gamma}(c/U)\cos\alpha$ is:

$$L_{\mathrm{LEV}} = -\rho\Gamma_{\mathrm{LEV}}\frac{U}{2} = \rho\dot{\Gamma}c\cos\alpha \approx \frac{1}{2}\rho U^2 c\, k^2 \cos\alpha. \tag{21}$$

Unfortunately also this expression cannot be generalised because we do not have a predictive model for how long LEVs

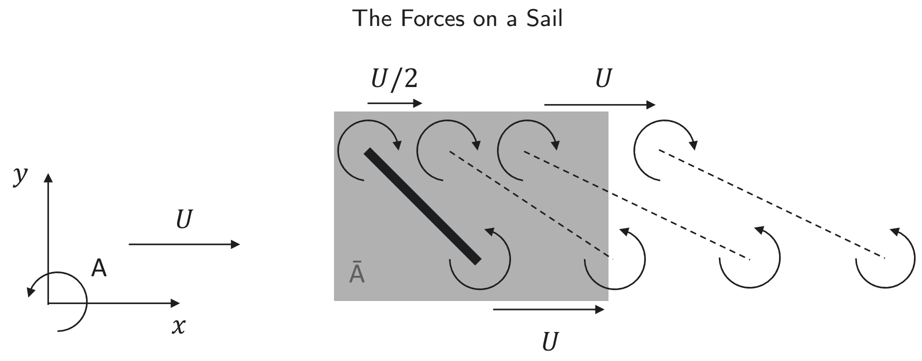

Figure 6: Vortex lift mechanism.

and TEVs travel at different velocities.

The relative velocity between LEVs and TEVs results, in a time averaged flow field, in more leading-edge vorticity than trailing edge vorticity around the plate. For example, the time-averaged results of Devoria and Mohseni (2017) on moderate incidence plates, show that the time-averaged leading-edge vorticity observed in the field of view (see FoV in Fig. 6) near the plate is about twice the trailing edge vorticity. Hence, by observing the time averaged flow field and considering as bound vorticity the net vorticity around the plate, including that of the separated shear layers, we can account for both the lift contributions L_b and L_{LEV}. This is discussed further in §7.

The relative velocity in the cross flow direction of the LEV with respect to the TEV is associated with a drag component. This is equivalent to a thickening or shrinking of the wake thickness between the leading and the trailing edge shear layers. Differently from the low incidence case (§3.1), the wake thickness is not negligible because of the leading-edge separation (Gault, 1957; Tani, 1964; Newman and Tse, 1992). At high incidences (§3.2), we considered the wake thickness as $d = k'c = 1.45$. At intermediate incidences $k' < 1.45$ because the wake thickness decreases to the flat plate boundary layer thickness as α tends to zero.

In summary, the lift and drag on a flat plate at moderate incidence can be associated with the vorticity production or with the vortex kinematics, but we do not have a model for either of these. For example, in contrast to the high incidence regime where the wake expands in the chordwise direction from c to d (Fig. 3), at moderate incidence it can either expand or shrink. Furthermore, the wake often stretches in the streamwise direction because counter-rotating vortices in the leading and trailing edge shear layers can travel at different speeds in the near wake.

It must be noted that the distinction between leading and trailing edge vorticity is unnecessary, and is used here only to distinguish between negative and positive vorticity, respectively. In fact, to compute the forces with eq. 5, the flow field must be described as an ensemble of vortex pairs with equal and opposite circulation. The choice of which positive vorticity is associated to which equal and opposite negative vorticity to form a vortex pair is arbitrary. Hence, this allows the force associated with the dynamics of any vorticity in the flow field to be estimated.

4. Three-dimensional Flow

In a three-dimensional space, the corresponding expression for eq. 5 is (Wu et al., 2006)

$$\boldsymbol{F} = \rho \Sigma_j (\dot{\Gamma}_j^+ A_j + \Gamma_j^+ \dot{A}_j)\, \boldsymbol{n}_j, \tag{22}$$

where the vorticity field is considered to be made of a combination of vortex rings, each with absolute strength Γ_j^+, minimum surface area spanned by the vortex loop A_j, and unit vector $\boldsymbol{n}_j$ normal to the surface and pointing in the opposite direction to its axial induced velocity. The superscript $^+$ is used to note that the circulation must be taken positive. The product $\rho\, \Gamma^+ A\, \boldsymbol{n}$ is the impulse of a vortex ring (Milne-Thomson, 1958).

Here we propose an alternative three dimensional form of eq. 22, where the total force on the body is the integral of the two-dimensional forces in the three Cartesian planes ($i = 1, 2, 3$):

$$\boldsymbol{F} = \frac{1}{2} \rho \Sigma_i (\dot{\boldsymbol{\Gamma}}_i \times \boldsymbol{d}_i + \boldsymbol{\Gamma}_i \times \dot{\boldsymbol{d}}_i), \tag{23}$$

where the summation Σ is intended as a vectorial sum. The $1/2$ factor is due to the fraction in front of the bracket on the right hand side of eq. 3. The vorticity must be considered in all of the three planes. For example, consider planes orthogonal to the x axis and compute the force $\boldsymbol{F}_{\boldsymbol{yz}}(x)$ based on the vorticity observed on that plane. Then integrate $\boldsymbol{F}_{\boldsymbol{yz}}(x)$ along x. Repeat the same procedure for planes orthogonal to the y and the z axes to find the forces $\boldsymbol{F}_{\boldsymbol{xz}}(y)$ and $\boldsymbol{F}_{\boldsymbol{xy}}(z)$. The total force is

$$\boldsymbol{F} = \frac{1}{2} \left(\int \boldsymbol{F}_{\boldsymbol{yz}}(x)\, \mathrm{d}x + \int \boldsymbol{F}_{\boldsymbol{xz}}(y)\, \mathrm{d}y + \int \boldsymbol{F}_{\boldsymbol{xy}}(z)\, \mathrm{d}z \right). \tag{24}$$

An example of how to implement eq. 22 and 24 is provided in the following sections (§4.1 and 4.2).

4.1. 3D Plate at Low Incidence

Consider a plate with a chord c and span b at a small angle of attack α. The reference system $O(x, y, z)$ is placed at the leading edge at one end of the span, and has directions $\boldsymbol{i}, \boldsymbol{j}, \boldsymbol{k}$ in the drag, lift, and span directions respectively (Fig. 7). The plate forms a vortex ring enclosed between

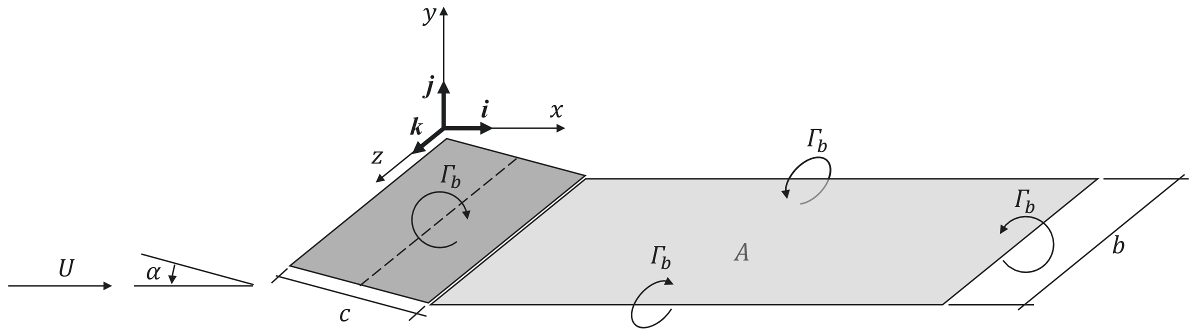

Figure 7: 3D plate at low incidence.

the plate's bound vortex, the two tip vortices and the starting vortex. The strength of the vortex ring is constant and equal to the bound vorticity, i.e. $\Gamma^+ = -\Gamma_b$, and no further vortex rings are formed, i.e. $\dot{\Gamma}^+ = 0$. The projection of the surface area of the vortex ring on the $y = 0$ plane increases along the x-direction at a rate $\dot{A}_y = Ub$. We considered the projected area because the vortex ring is at an angle with respect to the free stream. In fact, due to their reciprocal induced velocities, the tip vortices convect along the y-direction with a negative velocity V (with $|V| \ll |U|$), which is the downwash velocity. Therefore, the surface area of the vortex ring increases in the y-direction at a rate $\dot{A}_x = -Vb$. Substituting these results into eq. 22, we find

$$L = \rho\Gamma^+\dot{A}_y = -\rho U\Gamma_b b, \tag{25}$$

$$D = -\rho\Gamma^+\dot{A}_x = \rho V\Gamma_b b, \tag{26}$$

and, in non dimensional form,

$$C_L = -2\frac{\Gamma_b}{Uc}, \tag{27}$$

$$C_D = 2\frac{V}{U}\frac{\Gamma_b}{Uc}. \tag{28}$$

These lift and drag results (eq. 25 and 26) are consistent with lifting line theory (Milne-Thomson, 1958) and were independently derived by Lanchester (1907) and Prandtl (1918). They provide accurate results at small angles of incidence, where there is no leading-edge separation.

As mentioned above, it is less commonly appreciated that the same results can be achieved from eq. 24, which becomes

$$\boldsymbol{F} = \frac{1}{2}\left(\int_0^{c'} \boldsymbol{F_{yz}}(x)\,\mathrm{d}x + \int_0^{b} \boldsymbol{F_{xy}}(z)\,\mathrm{d}z\right), \tag{29}$$

where $c' = c\cos\alpha$. This formulation allows the use of the results of the 2D analysis. $\boldsymbol{F_{xy}}$ is the two-dimensional force on planes parallel to the (x, y) plane, whilst $\boldsymbol{F_{yz}}$ is the two-dimensional force on planes parallel to the (y, z) plane. Both forces can be computed with eq. 5. $\boldsymbol{F_{xy}}$ was computed in §3.1 and is given by eq. 8. $\boldsymbol{F_{yz}}$ can be computed noting that vorticity must be produced at the two tips at a rate $\dot{\Gamma}_b = \Gamma_b U/c'$ to allow the tip vortices to lengthen. Substituting this result together with eq. 8 into eq. 29, we find

$$L = -\frac{\rho}{2}\left((\Gamma_b U/c')bc' + U\Gamma_b b\right) = -\rho U\Gamma_b b, \tag{30}$$

which is the same result as eq. 25.

It is important to note that, for every vortex ring, the two integrals in eq. 29 give the same result, and thus it is sufficient to solve only one of the two integrals. Consider, for example, a rectangular vortex ring with area parallel to the wing. If the legs of the ring parallel to the span are pulled apart, the other two legs parallel to the tips must lengthen. On the plane $z = b/2$, we would observe an LEV and a TEV being pulled apart, while on the plane $x = c'/2$ we would observe vorticity being produced to lengthen the legs parallel to the tips. The force per unit length associated with pulling the two legs apart is $\boldsymbol{F_{xy}}$ (in the second integral of eq. 29), and this is equal to the force per unit length associated with the lengthening of the legs parallel to the tips, which is $\boldsymbol{F_{yz}}$ (in the first integral of eq. 29). The important consequence of this is that the three-dimensional solution, eq. 30, gives the same force per unit span as the two-dimensional solution, eq. 8.

In §3.1, it was noted that the drag of a plate at low incidence is approximately zero (eq. 9). However, in 3D there is a downwash velocity V, which is the relative y-velocity component between the bound and the starting vortex. Hence, $\boldsymbol{F_{xy}}$ is a vortex force $D = -\rho V\Gamma_b$. $\boldsymbol{F_{yz}}$ is associated with the vorticity produced at the two tips at a rate $\dot{\Gamma}_b = -\Gamma_b V/c'$ to allow the tip vortices to lengthen along the y-direction. Note that vorticity of the opposite sign is produced at the same rate at the two tips. Substituting these two results into eq. 29, we find

$$D = \frac{\rho}{2}\left((\Gamma_b V/c')bc' + V\Gamma_b b\right) = \rho V\Gamma_b b, \tag{31}$$

which is the same result as eq. 26.

The Forces on a Sail

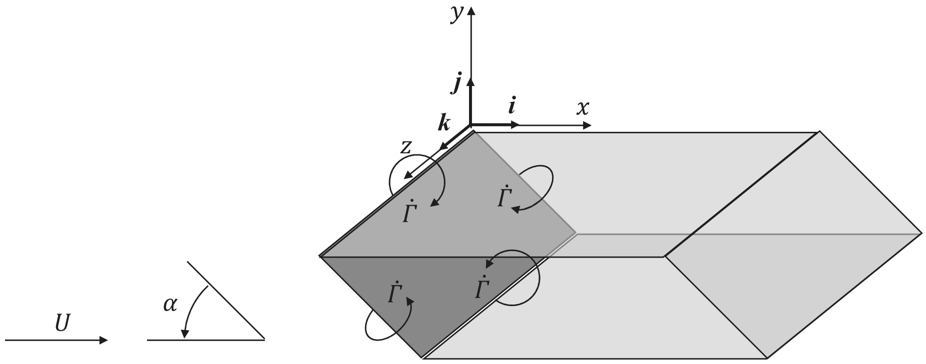

Figure 8: 3D plate at high incidence.

4.2. 3D Plate at High Incidence

Consider a plate at high incidence. The vorticity produced from the perimeter of the wing forms a vortex ring (Fig. 8). The direction orthogonal to the vortex ring is the plate-normal direction, defined by the unit vector $\boldsymbol{n}_\perp$ (which is approx. $\boldsymbol{i}$). The continuous production of vorticity results in new vortex rings being continuously formed and shed downstream.

Equation. 22 becomes

$$\boldsymbol{F} = \rho \dot{\Gamma}^+ A \boldsymbol{n}_\perp. \tag{32}$$

This force is made up of two components in the lift and drag directions, namely

$$L = \rho \dot{\Gamma}^+ A \cos\alpha, \tag{33}$$

$$D = \rho \dot{\Gamma}^+ A \sin\alpha, \tag{34}$$

and in non dimensional form,

$$C_L = 2\frac{\dot{\Gamma}^+}{U^2}\cos\alpha, \tag{35}$$

$$C_D = 2\frac{\dot{\Gamma}^+}{U^2}\sin\alpha. \tag{36}$$

Assuming $\dot{\Gamma}^+ = U_{SL}^2/2$ as in eq. 14 with $U_{SL} \approx U$, this formulation gives $C_L = 0$ and $C_D = 1$ for $\alpha = \pi/2$. This is consistent with flat plate experiments (White, 2011), where C_D decreases from 2 for an infinite aspect ratio to 1.5, 1.2 and 1.18 for a plate with aspect ratio 20, 5 and 2, respectively. It is noted that White (2011) states that these results are valid for Reynolds numbers of at least 10^4.

This result can be refined by accounting that the shear layer velocity is higher than the free stream velocity ($U_{SL} > U$) and that the wake thickness increases along the streamwise direction, i.e. the growth of the surface area of the shed vortex ring $\dot{A}$. This is akin of the role of the coefficients k and k' for the two-dimensional case (§3.2).

The same results as above can be achieved by integrating the two-dimensional forces using eq. 24, which reduces to eq. 29 for the case considered. A force associated with the vorticity production, which is uniform along the perimeter of the plate, and a vortex force associated with the growth of the wake, i.e. of the area of the vortex ring, can be identified. For each of these two force components, the two integrals in eq. 29 are identical and, hence, the three-dimensional and two-dimensional formulations give the same force per unit span. Consider, for example, the force associated with the production of vorticity, which is associated with the dominant force generation mechanism for low aspect ratio plates and which is the only one considered in the generation of eq. 32. Because the vorticity is generated uniformly along the perimeter of the plate, eq. 29 becomes

$$L = -\frac{\rho}{2}\left(\dot{\Gamma}_b bc + \dot{\Gamma}_b cb\right)\cos\alpha = -\rho\dot{\Gamma}_b bc\cos\alpha, \tag{37}$$

$$D = -\frac{\rho}{2}\left(\dot{\Gamma}_b bc + \dot{\Gamma}_b cb\right)\sin\alpha = -\rho\dot{\Gamma}_b bc\sin\alpha, \tag{38}$$

which is the same result as eq. 32 (in fact, $\Gamma^+ = -\Gamma_b$ and $A = bc$).

5. Interaction Between two Lifting Surfaces

Consider two 2D plates at low incidence and, as an example, chose the relative position as representative of the jib and the mainsail while sailing upwind as in Fig. 9. The two plates operate at low incidence and the forces are mostly associated with their bound circulations. Because the vorticity production is negligible as long as the boundary layer is attached, the flow is inviscid everywhere except in the boundary layers of the two plates, whose integral of vorticity is the bound circulation. For this reason, inviscid flow codes are accurate in these flow conditions. Consider the bound circulation represented as a single vortex in the centre of the plate such that the whole potential flow field can be represented by a bound vortex in the centre of each plate.[1] The values of the

[1]The bound circulation could be more accurately placed at the quarter chord to ensure the correct pitch moment, and the Kutta condition should be applied at the collocation point located half chord downstream along the chord (Katz and Plotkin, 2001). However, this would be less intuitive and unnecessary for the present discussion.

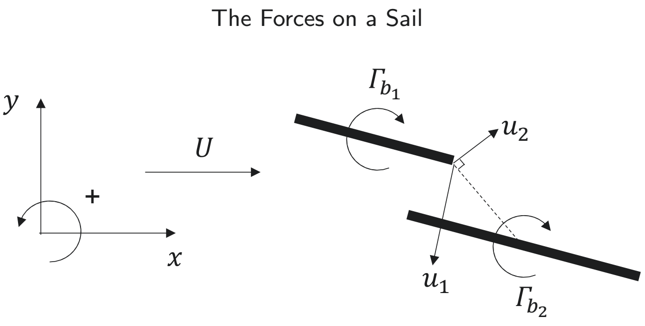

Figure 9: Interaction between two plates.

bound vortices are such as to ensure that the Kutta condition is satisfied at the trailing edge of the two plates.

Let us consider the effect of the back plate on the bound circulation of the front plate. In the absence of a second plate, it is shown in §3.1 that $\Gamma_b = -\pi U c \sin\alpha$. Conversely, the bound circulation Γ_{b2} of the back plate induces a plate-normal velocity at the trailing edge of the front plate that is opposite in sign to that induced by the bound circulation Γ_{b1} of the front plate. Therefore, to ensure that the Kutta condition is satisfied, the circulation of the front plate is higher in the presence of the back plate ($\Gamma_{b1} > \Gamma_b$). Vice versa, the plate-normal induced velocities due to the two bound circulations have the same sign at the trailing edge of the back plate. Therefore, Γ_{b2} is decreased by the effect of Γ_{b1}.

This result was explained by Gentry (1971, 1973) for the case of two sails. He noted that the circulation of the front sail (e.g. the jib) is enhanced by the presence of the back sail (e.g. the mainsail), and the circulation of the back sail is diminished by the presence of the front sail. There are only two conditions when this is not true. First, when there is significant overlap between the two sails (e.g. when a large *genoa* is used instead of a *jib*), such that the induced velocity u_2 has a positive component along u_1. Second, when the presence of the front sail prevents the back sail from stalling. In this case, if the front surface was removed, the circulation of the back sail would not increase but drop.

6. Effect of Free Vorticity on the Force

In the previous section (§5), the back plate was modelled as a discrete vortex with circulation Γ_{b2} and the effect of this vortex on the front plate was discussed. It is therefore natural to extend this analysis to the effect that any free vortex in the flow field has on an isolated plate. Hence, in this section, the effect of free vortices outside of the boundary layer on the force generation is discussed. To investigate, a generic velocity and vorticity fields that could represent the result of a numerical simulation or of flow visualisation are considered. In the following section (§6.1) this flow field is derived analytically for convenience, but the aim of this section is to provide guidelines on how *measured* or *computed* flow fields can be interpreted.

It must be emphasised that the proposed approach based on lumped vortices is a discrete representation of a continuous vorticity field. Hence, in the present discussion, vortices can be intended as the integral of the vorticity within any region of the fluid domain. For example, Pitt Ford and Babinsky (2013) and Arredondo-Galeana and Viola (2018) considered a stalled plate in 2D laminar flow conditions, and a stalled 3D wing in turbulent flow conditions, respectively. They measured the velocity field with particle image velocimetry and used the vortex detection criterion γ_2 (Graftieaux et al., 2001) to identify coherent vortical structures. They lumped all the vorticity measured in the flow field into the centroid of these vortical structures, and reconstructed the velocity field through a potential flow model with irrotational vortices. This allowed considering the force associated with the vorticity in different regions of the fluid domain.

6.1. The Flow Field Around a Circular Arc with a Free Vortex

Consider a circular arc, as an example of lifting surface, and compute the bound vorticity that is necessary to ensure the Kutta condition through a Kutta-Joukowsky transformation (Katz and Plotkin, 2001). The flow field around a cylinder is achieved by combining a free stream velocity U and a doublet. Add a vortex with circulation Γ_b at the centre of the cylinder (Fig. 10), which is taken to have radius R. The centre of the cylinder is placed in a complex coordinate reference system at $\zeta_0 = \mu i$, such that the transformed cylinder is a curved plate with maximum camber 2μ. The resulting potential flow field describes the flow around a plate with circulation Γ_b.

Add a free vortex with circulation Γ_v outside of the cylinder, at the complex coordinate $\zeta_v = \rho_v e^{i\tau_v} + \mu e^{i\pi/2}$, where ρ_v and τ_v are the radial and azimuthal coordinate of the vortex, respectively. The vortex has a mirror vortex inside the cylinder at $\zeta_v' = (R^2\rho_v^{-1})e^{i\tau_v} + \mu e^{i\pi/2}$ to maintain the non-penetration condition on the cylinder surface. The sum of the vortices inside the cylinder represent the integral of the vorticity in the boundary layer. We want this to be Γ_b, and therefore add an additional vortex Γ_v in the centre of the cylinder. The combined effect of $-\Gamma_v$ at the image vortex location and Γ_v in the centre of the vortex is simply to redistribute the total amount of vorticity Γ_b within the boundary layer.[2] The

[2] With the proposed approach, which is the same as in Pitt Ford and Babinsky (2013), we consider the bound vortex and the external vortex as separate identities. For example, the external vortex could be a vortex gust. It should be noted that an alternative approach is to consider the external

overall complex potential is (Arredondo-Galeana and Viola, 2018)

$$F(\zeta) = U(\zeta-\zeta_0)e^{-i\alpha} + \frac{UR^2e^{i\alpha}}{(\zeta-\zeta_0)} - \frac{i(\Gamma_b+\Gamma_v)}{2\pi}\ln(\zeta-\zeta_0) - \frac{i\Gamma_v}{2\pi}\ln\frac{\zeta-\zeta_v}{\zeta-\zeta'_v}. \tag{39}$$

The complex velocity in the cylinder plane is given by differentiating the complex potential with respect to ζ, that is

$$W(\zeta) = \frac{dF(\zeta)}{d\zeta} = Ue^{-i\alpha} - \frac{UR^2e^{i\alpha}}{(\zeta-\zeta_0)^2} - \frac{i(\Gamma_b+\Gamma_v)}{2\pi}\frac{1}{\zeta-\zeta_0} - \frac{i\Gamma_v}{2\pi}\left[\frac{1}{\zeta-\zeta_v} - \frac{1}{\zeta-\zeta'_v}\right]. \tag{40}$$

The real and imaginary part of the complex velocity give the streamwise and cross-flow velocity components, respectively. The resulting flow field is showed in Fig. 11a. The cylinder plane can be mapped into the circular arc plane with the transformation $z = (\zeta + R\zeta^{-2})e^{-i\alpha}$ (Fig. 11b). The bound circulation that ensures the Kutta condition is found by the additional condition that the point on the cylinder corresponding to the trailing edge, $\zeta_{TE} = R\,e^{-i\beta} + i\mu = 0$, is a stagnation point, i.e. $W(\zeta_{TE}) = 0$.

Solving eq. 40 for Γ_b gives an expression for the bound circulation as a function of the circulation and position of the external vortex:

$$\Gamma_b = -4R\pi U\sin(\alpha+\beta) - \kappa\Gamma_v, \tag{41}$$

where $\beta = \mathrm{atan}(4\mu/c)$ is the effective angle of attack due to the plate curvature, and

$$\kappa = 2R\frac{R-\rho_v\cos(\beta+\tau_v)}{R^2+\rho_v^2-2R\rho\cos(\beta+\tau_v)}. \tag{42}$$

The first term on the right hand side of eq. 41 is the value that the bound circulation would have without the external vortex. Because it is negative, it is associated with a positive lift. The presence of the external vortex modifies the bound circulation by the coefficient κ, which depends on the spatial location of the vortex with respect to the circular arc. The contours of κ in the cylinder and circular arc planes are shown in Fig. 11a and b, respectively. The effect of the external vortex on the force generation is discussed in the next two sections (§6.2 and 6.3).

6.2. Effect of a Free Vortex on the Force

The flow field described in §6.1 is made of two vortices: the external vortex and a vortex with circulation Γ_b representing the overall vorticity in the boundary layer. The force

vortex as vorticity that was in the boundary layer such as, for example, in Corkery et al. (2019). In this latter case, the additional vortex Γ_v is no longer added in the centre of the cylinder, Γ_b is the vorticity that was originally in the boundary layer, while $\Gamma_b - \Gamma_v$ is the remaining vorticity in the boundary layer after Γ_v has been shed.

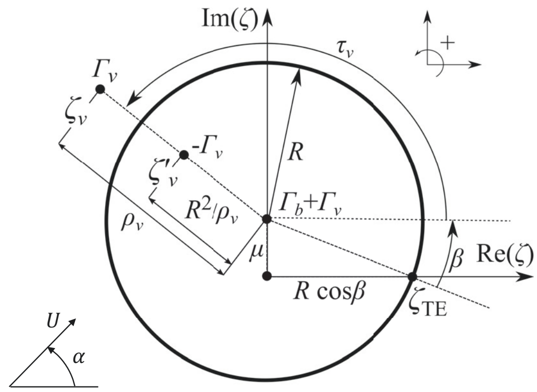

Figure 10: Complex plane of a rotating cylinder with an external vortex.

generation is associated with the kinematics of vortex pairs that can be arbitrary chosen as long as all the circulation is accounted for and that the net circulation is zero to satisfy Kelvin's theorem.

Because the net observable vorticity is $\Gamma_b + \Gamma_v \neq 0$, then there must be circulation with equal magnitude and opposite sign somewhere far away along the wake. For example, consider the vortex pair made of Γ_b in the boundary layer and $-\Gamma_b$ infinite downstream, and the vortex pair made of Γ_v near the circular arc and $-\Gamma_v$ infinitely downstream. The force is associated with the change in size and orientation of these two vortex pairs.

The bound circulation is moving away from the starting vortex at velocity U, thus leading to the Kutta-Joukowsky lift (eq. 8): $L_b = -\rho U\Gamma_b$. The contribution of the free vortex is not as straightforward because its velocity depends on its position. If we use this approach to interpret the results of a numerical or experimental flow field, a critical distinction must be made.

If the flow is instantaneous, the velocity of the circulation Γ_v could be approximated by the average velocity in the region occupied by the vorticity (better if the average is weighted by the distribution of vorticity). Its force contribution is zero only if the free vortex convects downstream with velocity U, which is equivalent to the convection of the vortex pair being frozen. For example, consider the circular arc being a yacht sail. If the free vortex was a vortex gust in turbulent wind and its trajectory was unchanged by the sail, it would have no force contribution. Conversely, if the free vortex is close enough to the sail such that the velocity induced by the bound circulation on the free vortex is not negligible, then the vortex pair would be modified giving rise to a gust force.

Therefore, if the streamwise velocity of a vortex with positive circulation is higher than U, it is associated with a positive lift, and vice versa if the circulation is negative (e.g. the LEV in eq. 21). When the cross-flow velocity in the y-direction (with reference to Fig. 10b) of a vortex with positive circulation is positive, it is associated with thrust, and with drag if the circulation is negative.

The Forces on a Sail

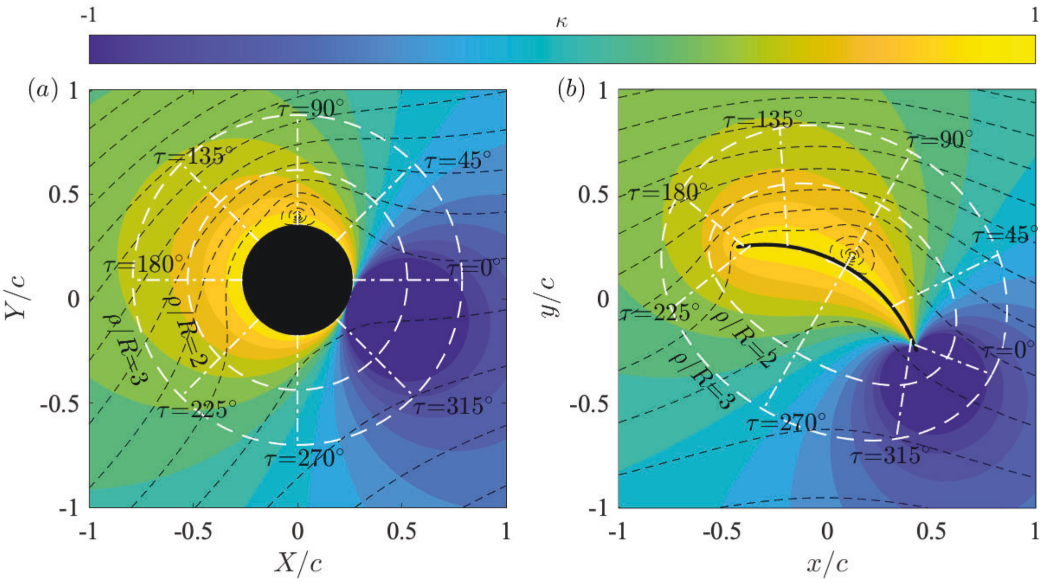

Figure 11: Contour of κ on the cylinder plane ζ (a) and the circular arc plane z. White dotted lines show the radial and azimuthal coordinates ρ and τ. Black dotter lines show an example of streamlines for the arbitrary set of values $\Gamma_b/(cU) = 0.26$, $\Gamma_v/(cU) = 2.5$, $\rho/R = 1.15$ and $\tau = \pi/2$.

6.3. Effect of a Free Vortex on the Bound Circulation

The effect of the free vortex on the bound circulation can be deduced from equations 41 and 42. The addition of free vorticity in the surrounding fluid contributes with an induced velocity at the trailing edge, thus resulting in a different value of the bound circulation. If the free vortex is on the lifting surface, then $\kappa = 1$ and the bound circulation is reduced precisely by the free vortex circulation (Fig. 11). Its effect decreases with increasing distance from the lifting surface.

Consider, for example, a realistic flow field with leading-edge separation and time averaged reattachment. The vorticity in the LEV contributes to the generation of induced velocity at the trailing edge and thus the bound circulation must be lower than it would have been without LEV. Therefore, while the LEV provides a positive lift contribution (see eq. 21), it also leads to a lower bound circulation. The sum of the two effects cancel out each other perfectly if the LEV remains in a fixed position with respect to the lifting surface and at position $\kappa \approx 1$ (e.g. see the trapped vortex discussed by Saffman and Sheffield, 1977). The lift enhancing mechanism of the LEV, firstly observed by Ellington et al. (1996) and then well documented by many others (Birch and Dickinson, 2001; Muijres et al., 2008; Lentink and Dickinson, 2009; Lentink, 2011; Videler, 2004; Harbig et al., 2013; Wong and Rival, 2015; Nabawy and Crowther, 2017; Linehan and Mohseni, 2020), is referred to the difference in lift between a wing with LEV and a wing otherwise stalled. In fact, the main role of the LEV is to retain leading-edge vorticity near the lifting surface instead of letting it convect downstream at the freestream velocity.

7. Forces from Time-Averaged Flow Fields

If the flow field is time averaged, the velocity of any observed vorticity is null. Hence, equation eq. 5 or 23 cannot be used because $\dot{\boldsymbol{d}}$ cannot be observed. However, it is noted that time-averaged vorticity around the solid body is, on average, moving with the body. Therefore, the Kutta-Joukowsky lift formula holds also for a time-averaged flow field where the bound circulation is the integral of all of the observed time-averaged vorticity within a region including the solid body and intersecting its wake orthogonally. The lift contribution of the vorticity production and of the vortex lift contribution of repeatedly shed vortices is not neglected but is implicitly included. In fact, the lower the flow velocity convecting vorticity through an arbitrary volume, the higher the time averaged value of vorticity in the volume.

The time-averaged drag can be estimated using Taylor's formula (Taylor's Appendix in Bryan et al., 1925),

$$D = \int_W (p - p_0)\,\mathrm{d}y, \tag{43}$$

which states that the drag is the integral over a line W intersecting the wake orthogonally, of the difference between the pressure in the wake p and that in the far field p_0. By using the Bernoulli equation, it is found that Taylor's formula shows that the drag is equal to the momentum loss in the wake, a result directly verifiable by applying Newton's second law. Wu et al. (2006) recently showed that the first order approximation of eq. 43 is

$$D = -\rho U \int_W y w\,\mathrm{d}y, \tag{44}$$

thus enabling the use of Taylor's formula by knowledge of only the vorticity field along W. For example, a two-dimensional plate with chord c at incidence α that generates vorticity at a rate $\dot{\Gamma}$, forms two shear layers with strength $\gamma = \dot{\Gamma}/U$ that extend from each edge of the plate to infinity. The shear layers are the only vorticity that intersects W and thus eq. 44 becomes

$$D = \rho U \gamma c \sin\alpha = \rho \dot{\Gamma} c \sin\alpha. \tag{45}$$

Substituting $\gamma = \dot{\Gamma}/U$ into eq. 45, gives precisely eq. 17.

Liu et al. (2015) show that eq. 44 is equivalent to Filon's drag formula when the shear layer approximation $\partial/\partial y \gg \partial/\partial x$ is used. Therefore, eq. 44 is a form of the Filon's formula that, together with the Kutta-Joukowsky formulation, allows the computation of the time-averaged lift and drag.

These two equations together, that we call the Kutta-Joukowsky-Filon equations, can be combined into one vectorial equation and extended to three-dimensional flow as (Liu et al., 2017)

$$\boldsymbol{F} = \rho \boldsymbol{U} \times \boldsymbol{\Gamma_b} + \rho \boldsymbol{U} Q, \tag{46}$$

where

$$Q = \frac{1}{n_d - 1} \int_{S_W} (z\omega_y - y\omega_z)\, \mathrm{d}S, \tag{47}$$

$n_d = 2$ and 3 in two and three dimensions, respectively. S_W is a plane orthogonally intersecting the wake. For example, for a plate with span b and chord c at incidence α, eq. 46 becomes

$$\boldsymbol{F} = \rho U \Gamma_b b\, \boldsymbol{j} + \rho U \gamma b c \sin\alpha\, \boldsymbol{i}. \tag{48}$$

Noting that $\gamma = \dot{\Gamma}/U$, this result is consistent with eq. 25 and 34.

8. Conclusions

Force generation on fins, wings, blades and sails have been traditionally explained through thin airfoil theory and lifting line theory. However, the underlying assumptions of these theories are not compatible with separated flow. Therefore, a new paradigm is proposed, that is compatible with both attached and separated flow conditions, and both streamlined and bluff bodies.

Based on the impulse theory, this paradigm enables an intuitive and in-depth understanding of some of the key results of thin airfoil theory and lifting line theory. In addition, it provides an intuitive interpretation of how a region of vorticity in the flow field is associated with a force contribution. Hence, the proposed approach can guide designers of lifting surfaces by providing quantitative objectives based on the observed flow field.

The proposed paradigm is as follows. To ensure the non-slip and non-penetration condition, the sail must generate vorticity. The vorticity in the boundary layer is exactly what is needed to ensure these two conditions. The Kutta condition and Kelvin's theorem set two further conditions that make this vorticity field completely determined, both in the boundary layer and infinitely far from the solid body. This vorticity field can be described as an ensemble of vortex rings, which degenerate in vortex pairs in two dimensions. The force on the solid body associated with each vortex ring is the rate of change of their impulse $\boldsymbol{I}$:

$$\boldsymbol{F} = \rho \frac{\mathrm{d}\boldsymbol{I}}{\mathrm{d}t} = \rho \left(\dot{\Gamma}^+ A + \Gamma^+ \dot{A} \right) \boldsymbol{n}, \tag{49}$$

There are three mechanisms by which the impulse can be changed: (1) generating new vortex rings at a rate $\dot{\Gamma}^+$; (2) varying the area of the vortex ring at a rate $\dot{A}$; (3) rotating the vortex ring and thus the orientation of $\boldsymbol{n}$.

1. The first mechanism is that of bluff bodies such as parachutes, whose continuous generation of vortex rings parallel to the parachute surface results in a drag per unit span that is $D = \rho \dot{\Gamma}^+ A$. When the vorticity is generated along a perimeter that does not entirely lies on a plane orthogonal to the stream, this force contribution has both a lift and a drag component.
2. The second mechanism is that of streamlined bodies such as an airplane wing at low incidence. The vortex ring is enclosed between the wing of span b, the tip vortices and the starting vortex. The area of the vortex ring increases at a rate $\dot{A} = Ub$, resulting in a lift per unit span $L = \rho U \Gamma$.
3. Any vortex ring in the fluid such as, for instance, the parachute-type vortex ring generated around the perimeter of a solid body, might change shape and orientation. For any plane intersecting the ring, the vortex force per unit depth is proportional to the $\rho \delta_U \Gamma$, where δ_U is the difference in velocity between the legs of the vortex ring.

Based on this paradigm, the knowledge of the instantaneous vorticity and velocity field allows the computation/interpretation of the instantaneous lift and drag. Moreover, it is also shown that the time-averaged vorticity field alone is sufficient to compute/interpret the time-averaged lift and drag by using the Kutta-Joukowsky-Filon equation.

Acknowledgements

This paper is dedicated to Arvel Gentry, whose dedication to public outreach inspired generations of sail aerodynamicists. The authors are deeply grateful to Prof. William Graham, University of Cambridge, for his insightful comments and for the generosity with which he has shared his in-depth knowledge on this subject. The authors are also very grateful to the anonymous Reviewers, whose comments enabled the paper to be greatly enhanced.

References

A. R. Claughton, Shenoi, R.A., Wellicome, J.F., 1998. Sailing Yacht Design: Theory. First ed., Addison Wesley Longman.

The Forces on a Sail

Afgan, I., McNaughton, J., Rolfo, S., Apsley, D., Stallard, T., Stansby, P., 2013. Turbulent flow and loading on a tidal stream turbine by LES and RANS. Int. J. Heat Fluid Flow 43, 96–108. URL: http://linkinghub.elsevier.com/retrieve/pii/S0142727X13000672, doi:10.1016/j.ijheatfluidflow.2013.03.010.

Akkala, J.M., Buchholz, J.H.J., 2017. Vorticity transport mechanisms governing the development of leading-edge vortices. J. Fluid Mech. 829, 512–537. doi:10.1017/jfm.2017.559.

Arena, A.V., Mueller, T.J., 1980. Laminar Separation, Transition, and Turbulent Reattachment near the Leading Edge of Airfoils. AIAA J. 18, 747–753. doi:10.2514/3.50815.

Arredondo-Galeana, A., Viola, I.M., 2018. The leading edge vortex of yacht sails. Ocean Eng. Virtual Spec. Issue Yacht Eng. 2017 , 11URL: https://doi.org/10.1016/j.oceaneng.2018.02.029, doi:10.1016/j.oceaneng.2018.02.029.

Babinsky, H., Stevens, P.R.R.J., Jones, A.R., Bernal, L.P., Ol, M.V., 2016. Low Order Modelling of Lift Forces for Unsteady Pitching and Surging Wings ., in: 54th AIAA Aerosp. Sci. Meet. AIAA SciTech Forum, (AIAA 2016-0290), pp. 1–12.

Basu, B.C., Hancock, G.J., 1978. The unsteady motion of a two-dimensional aerofoil in incompressible inviscid flow. Commun. Pure Appl. Math. 87, 159–178.

Birch, J.M., Dickinson, M.H., 2001. Spanwise flow and the attachment of the leading-edge vortex on insect wings. Nature 412, 729–733. doi:10.1038/35089071.

Bot, P., 2019. Force Variations Related to Flow Pattern Changes Around a High-Camber Thin Wing. AIAA J. , 1–7doi:10.2514/1.J058443.

Bot, P., Rabaud, M., Thomas, G., Lombardi, A., Lebret, C., 2016. Sharp Transition in the Lift Force of a Fluid Flowing Past Nonsymmetrical Obstacles: Evidence for a Lift Crisis in the Drag Crisis Regime. Phys. Rev. Lett. 117, 234501. URL: https://link.aps.org/doi/10.1103/PhysRevLett.117.234501, doi:10.1103/PhysRevLett.117.234501.

Bot, P., Viola, I.M., Flay, R.G.J., Brett, J.S., 2014. Wind-tunnel pressure measurements on model-scale rigid downwind sails. Ocean Eng. 90, 84. doi:10.1016/j.oceaneng.2014.07.024.

Bryan, L.W., Williams, D.H., Taylor, G.I., 1925. An Investigation of the Flow of Air Around an Airfoil of Infinite Span. Phil. Trans. R. Soc. Lond. A 225, 199–245.

Carter, J.E., Vatsa, V.N., 1984. Analysis of Airfoil Leading Edge Separation. Technical Report. United Technologies Research Center.

Chang, P.K., 1970. Separation of Flow, in: Sep. Flow, pp. 452–530. doi:10.1016/b978-0-08-013441-3.50013-7.

Chowdhury, J., Ringuette, M.J., 2019. A simple vortex-loop-based model for unsteady rotating wings. J. Fluid Mech. 880, 1020–1035. doi:10.1017/jfm.2019.735.

Collie, S.J., Jackson, P.S., Fallow, J.B., Gerritsen, M., B, F.J., 2009. Two-dimensional CFD-based parametric analysis of downwind sail designs. Int. J. Small Cr. Technol. 151, 15. doi:10.3940/rina.ijsct.2004.b1.19041.

Corkery, S.J., Babinsky, H., 2018. Force Production Mechanisms for a Flat Plate Wing at Low Reynolds Numbers. 2018 AIAA Aerosp. Sci. Meet. , 1–13URL: https://arc.aiaa.org/doi/10.2514/6.2018-0816, doi:10.2514/6.2018-0816.

Corkery, S.J., Babinsky, H., Graham, W.R., 2019. Quantification of added-mass effects using particle image velocimetry data for a translating and rotating flat plate. J. Fluid Mech. 870, 492–518. URL: https://www.cambridge.org/core/product/identifier/S0022112019002313/type/journal{_}article, doi:10.1017/jfm.2019.231.

Crompton, M.J., Barrett, R.V., 2000. Investigation of the separation bubble formed behind the sharp leading edge of a flat plate at incidence. Proc. Inst. Mech. Eng. Part G J. Aerosp. Eng. 214, 157–176. URL: http://pig.sagepub.com/lookup/doi/10.1243/0954410001531980, doi:10.1243/0954410001531980.

Cyr, S., Estelle, J., 1992. A theoretical Model for Flow about a circular-arc Aerofoil with Separation Thesis by. Ph.D. thesis. McGill University.

Deparday, J., Augier, B., Bot, P., 2018. Experimental analysis of a strong fluid-structure interaction on a soft membrane-Application to the flapping of a yacht downwind sail. J. Fluids Struct. 81, 547–564.

Devoria, A.C., Mohseni, K., 2017. On the mechanism of high-incidence lift generation for steadily translating low-aspect-ratio wings. J. Fluid Mech. 813, 110–126. doi:10.1017/jfm.2016.849.

Dugan, J.P., Cisotti, S., 1970. A free-streamline model of the two-dimensional sail. J. Fluid Mech. 42, 433–446. URL: http://journals.cambridge.org/download.php?file=/FLM/FLM42{_}03/S0022112070001398a.pdf{&}code=3af0682f566e69c90e7fa9d615b280fd, doi:10.1017/S0022112070001398.

Eldredge, J.D., 2019. Mathematical Modeling of Unsteady Inviscid Flows. Springer.

Eldredge, J.D., Jones, A.R., 2019. Leading-Edge Vortices: Mechanics and Modeling. Annu. Rev. Fluid Mech. , 75–104URL: https://doi.org/10.1146/annurev-fluid-010518-, doi:10.1146/annurev-fluid-010518.

Ellington, C.P., van den Berg, C., Willmott, A.P., Thomas, A.L.R., 1996. Leading edge vortices in insect flight. Nature 384.

ESDU, S., 1970. Fluid Forces and Moments on Flat Plates. Data Item 70015. Eng. Sci. Data Unit, London, UK .

Fage, A., Johansen, F.C., 1927. On the Flow of Air behind an Inclined Flat Plate of Infinite Span. Proc. R. Soc. London A Math. Phys. Eng. Sci. 116, 170–197. URL: http://rspa.royalsocietypublishing.org/content/116/773/170, doi:10.1098/rspa.1927.0130.

Fage, A., Johansen, F.C., 1928. XLII. The structure of vortex sheets. London, Edinburgh, Dublin Philos. Mag. J. Sci. 5, 417–441. URL: https://doi.org/10.1080/14786440208564482, doi:10.1080/14786440208564482.

Filon, L.N.G., 1926. The forces on a cylinder in a stream of viscous fluid. Proc. R. Soc. London. Ser. A, Contain. Pap. a Math. Phys. Character 113, 7–27. doi:10.1098/rspa.1926.0136.

Flay, R.G.J., Piard, A., Bot, P., 2017. Aerodynamics of a highly cambered circular aerofoil: experimental investigation, in: Proc. 4th Innov'Sail Int. Conf. Innov. High Perform. Sail. Yachts, Lorient, France.

Fossati, F., 2009. Aerodynamics and the performance of sailing yacht. doi:10.1109/ISGT-Asia.2014.6873780.

Gault, D.E., 1957. An investigation at low speed of the flow over a simulated flat plate at small angles of attack using pitot-static and hot-wire probes. Natl. Advis. Comm. Aeronaut. .

Gentry, A., 1971. The Aerodynamics of Sail Interaction. Third AIAA Symp. AeroHydrodnautics Sail. , 1–12.

Gentry, A., 1973. More on the Slot Effect. Sail Mag. , 2–4.

Graftieaux, L., Michard, M., Grosjean, N., 2001. Combining {PIV}, {POD} and vortex identification algorithms for the study of unsteady turbulent swirling flows. Meas Sci Technol 12, 1422–1429. doi:10.1088/0957-0233/12/9/307.

Harbig, R.R., Sheridan, J., Thompson, M.C., 2013. Reynolds number and aspect ratio effects on the leading-edge vortex for rotating insect wing planforms. J Fluid Mech 717, 166–192. URL: http://journals.cambridge.org/abstract{_}S0022112013003352{%}5Cnhttp://www.journals.cambridge.org/abstract{_}S0022112013003352, doi:10.1017/jfm.2012.565.

von Helmholtz, H.L.F., 1868. Über discontinuierliche Flüssigkeitsbewegungen. Monatsberichte der Königlichen Akad. der Wissenschaften zu Berlin 23, 215–228.

Hoerner, S.F., Borst, H.V., 1975. Fluid-dynamic lift. Hoerner Fluid Dynamics, Bricktown New Jersey.

Huang, M.K., Chow, C.Y., 1986. Trapping of a free vortex by airfoils with surface suction. AIAA J. 24, 1217–1218. doi:doi:10.2514/6.1985-446.

Huang, Y., Venning, J., Thompson, M.C., Sheridan, J., 2015. Vortex separation and interaction in the wake of inclined trapezoidal plates. J. Fluid Mech. 771, 341–369. doi:10.1017/jfm.2015.160.

Joukowsky, N.E., 1906. On annexed vortices. Proc. Phys. Sect. Nat. Sci. Soc. 13, 12–25.

Katz, J., 1981. A discrete vortex method for non-steady separted flow over an airfoil. J. Fluid Mech. 102.

Katz, J., Plotkin, A., 2001. Low-Speed Aerodynamics. doi:10.1017/cbo9780511810329.

Kim, D., Gharib, M., 2011. Characteristics of vortex formation and thrust performance in drag-based paddling propulsion. J. Exp. Biol. 214, 2283–2291. URL: http://jeb.biologists.org/cgi/doi/10.1242/jeb.050716, doi:10.1242/jeb.050716.

von Kirchhoff, H.G., 1868. Zur Theorie freier Flüssigkeitsstrahlen. J. für Math. LXX, 289–298.

Kiya, M., Arie, M., 1977. A contribution to an inviscid vortex-shedding model to an inclined flat plate in uniform flow. J. Fluid Mech. 82, 223–240. doi:10.1017/S0022112077000627.

Koumoutsakos, P., Leonard, A., 1995. High-resolution simulation of the flow around an impulsively started cylinder using vortex methods. J. Fluid Mech. 296, 1–38.

Kutta, W.M., 1902. Auftreibskrafte in Stromenden Flussigkeiten. lilust. Aeronaut. Mitt. .

Lamb, H., 1932. Hydrodynamics.

Lanchester, F.W., 1907. Aerodynamics: constituting the first volume of a complete work on aerial flight. volume 1. London, A. Constable & Co., Ltd.

Larsson, L., Eliasson, R.E., 1995. Principles of yacht design. First amer ed., Society of Naval Architects & Marine Engineers.

Lee, J.J., Hsieh, C.T., Chang, C.C., Chu, C.C., 2012. Vorticity forces on an impulsively started finite plate. J. Fluid Mech. 694, 464–492. doi:10.1017/jfm.2011.563.

Lentink, D., 2011. Leading-Edge Vortices Elevate Lift of Autorotrating Plant Seeds. Science (80-.). 1438, 10–13. doi:10.1126/science.1174196.

Lentink, D., 2018. Accurate fluid force measurement based on control surface integration. Exp. Fluids 59, 1–12. URL: https://doi.org/10.1007/s00348-019-2838-7http://dx.doi.org/10.1007/s00348-017-2464-1, doi:10.1007/s00348-017-2464-1.

Lentink, D., Dickinson, M.H., 2009. Rotational accelerations stabilize leading edge vortices on revolving fly wings. J. Exp. Biol. 212, 2705–2719. URL: http://jeb.biologists.org/cgi/doi/10.1242/jeb.022269, doi:10.1242/jeb.022269.

Leonard, A., Roshko, A., 2001. Aspects of flow-induced vibrations. J. Fluids Struct. 15, 415–425.

Lighthill, J., 1986. An informal introduction to theoretical fluid mechanics. doi:10.1137/1030121.

Linehan, T., Mohseni, K., 2020. On the maintenance of an attached leading-edge vortex via model bird alula. URL: http://arxiv.org/abs/2001.03964, arXiv:2001.03964.

Liu, L.Q., Wu, J.Z., Su, W.D., Kang, L.L., 2017. Lift and drag in three-dimensional steady viscous and compressible flow. Phys. Fluids 29. doi:10.1063/1.4989747, arXiv:1611.09615.

Liu, L.Q., Zhu, J.Y., Wu, J.Z., 2015. Lift and drag in two-dimensional steady viscous and compressible flow. J. Fluid Mech. 784, 304–341. doi:10.1017/jfm.2015.584.

Lord Rayleigh, F.R.S., 1876. On the Resistance of Fluids. Philos. Mag. J. Sci. 2, 430–441.

Marzanek, M.F., Rival, D.E., 2019. Separation mechanics of non-slender delta wings during streamwise gusts. J. Fluids Struct. 90, 286–296. doi:10.1016/j.jfluidstructs.2019.07.001.

Maxworthy, T., 2007. The formation and maintenance of a leading-edge vortex during the forward motion of an animal wing. J. Fluid Mech. 587, 471–475. doi:10.1017/S0022112007007616.

Milgram, J.H., 1998. Fluid mechanics for sailing vessel design. Annu. Rev. Fluid Mech. 30, 613–653. URL: https://doi.org/10.1146/annurev.fluid.30.1.613, doi:10.1146/annurev.fluid.30.1.613.

Milne-Thomson, L.M., 1958. Theoretical Aerodynamics (4th Edition).

Muijres, F.T., Johansson, L.C., Barfield, R., Wolf, M., Spedding, G.R., Hedenström, A., Hedenstrom, A., 2008. Leading-Edge Vortex Improves Lift in Slow-Flying Bats. Science (80-.). 319, 1250–1253. URL: http://www.sciencemag.org/cgi/doi/10.1126/science.1153019, doi:10.1126/science.1153019.

Muir, R.E., Arredondo-galeana, A., 2017. The leading-edge vortex of swift wing-shaped delta wings. R. Soc. Open Sci. 4.

Nabawy, M.R.A., Crowther, W.J., 2017. The role of the leading edge vortex in lift augmentation of steadily revolving wings: a change in perspective. J. R. Soc. Interface 14, 20170159. URL: http://rsif.royalsocietypublishing.org/lookup/doi/10.1098/rsif.2017.0159, doi:10.1098/rsif.2017.0159.

Nava, S., Bot, P., Carter, J., Norris, S.E., Cater, J., Norris, S.E., 2016. Modelling the Lift Crisis of a Cambered Plate at 0 deg Angle of Attack, in: Proc. 20th Australas. Fluid Mech. Conf., Australasian Fluid Mechanics Society, Perth, Australia. pp. 6–9.

Newman, B.G., Tse, M.M.C., 1992. Incompressible flow past a flat plate aerofoil with leading edge separation bubble. Aeronaut. J. 96, 57–64. doi:10.1017/S0001924000024532.

Okamoto, M., Azuma, A., 2005. Experimental Study on Aerodynamic Characteristics of Unsteady Wings at Low Reynolds Number. AIAA J. 43, 3–6. doi:10.2514/1.14813.

van Oossanen, P., 2018. The Science of Sailing: Part 2. First edit ed., Van Oossanen Academy.

Owen, P., Klanfer, L., 1955. On the Laminar Boundary Layer Separation from the Leading edge of a Thin Aerofoil. Technical Report 220. Ministry of Supply. URL: http://naca.central.cranfield.ac.uk/reports/arc/cp/0220.pdf.

Phillips, W.F., 2004. Lifting-Line Analysis for Twisted Wings and Washout-Optimized Wings. J. Aircr. 41, 128–136. URL: https://doi.org/10.2514/1.262, doi:10.2514/1.262.

Pitt Ford, C.W., Babinsky, H., 2013. Lift and the leading-edge vortex. J. Fluid Mech. 720, 280–313. URL: http://www.journals.cambridge.org/abstract{_}S0022112013000281, doi:10.1017/jfm.2013.28.

Prandtl, L., 1918. Königliche Gesellschaft der Wissenschaften zu Göttingen. Tragflügeltheorie .

Regis, E., 2020. The Enigma of Aerodynamic Lift. Sci. Am. 322, 44–51. doi:10.1038/scientificamerican0220-44.

Richards, P.J., Viola, I.M., 2015. Leading edge vortex dynamics, in: 17th Australas. Wind Eng. Soc. Work.

Rival, D.E., van Oudheusden, B., 2017. Load-estimation techniques for unsteady incompressible flows. Exp. Fluids 58, 1–11. doi:10.1007/s00348-017-2304-3.

Roshko, A., 1954. On the drag and shedding frequency of two dimensional bluff bodies. NACA TN 3169 .

Roshko, A., 1955. On the Wake and Drag of Bluff Bodies. J. Aeronaut. Sci. 22, 124–132. URL: http://arc.aiaa.org/doi/10.2514/8.3286, doi:10.2514/8.3286.

Saffman, P.G., Sheffield, J.S., 1977. Flow over a Wing with an Attached Free Vortex. Stud. Appl. Math. 57, 107–117.

Sarpkaya, T., 1975. An inviscid model of two-dimensional vortex shedding for transient and asymptotically steady separated flow over an inclined plate. J. Fluid Mech. 68, 109–128. doi:10.1017/S0022112075000717.

Souppez, J.B.R.G., Arredondo-Galeana, A., Viola, I.M., 2019a. Recent Advances in Downwind Sail Aerodynamics. 23rd Cheasapeake Sail. Yacht Symp. .

Souppez, J.B.R.G., Arredondo-Galeana, A., Viola, I.M., 2019b. Recent Advances in Numerical and Experimental Downwind Sail Aerodynamics. J. Sail. Technol. 4, 45–65. URL: https://doi.org/.

Souppez, J.B.R.G., Bot, P., Viola, I.M., 2021. On the effect of the leading-edge separation bubble on the aerodynamics of spinnakers, in: 7th High Perform. Yacht Des. Conf., Auckland, New Zealand.

Stevens, P.R.R.J., Babinsky, H., Manar, F., Mancini, P., Jones, A.R., Granlund, K.O., Nakata, T., Phillips, N., Bomphrey, R.J., Gozukara, A.C., 2016. Low Reynolds Number Acceleration of Flat Plate Wings at High Incidence (Invited), in: 54th AIAA Aerosp. Sci. Meet. AIAA SciTech Forum, (AIAA 2016-0286), pp. 1–15. URL: https://doi.org/10.2514/6.2016-0286.

Stevenson, J.P.J., Nolan, K.P., Walsh, E.J., 2016a. Particle image velocimetry measurements of induced separation at the leading edge of a plate. J. Fluid Mech. 804, 278–297. doi:10.1017/jfm.2016.532.

Stevenson, J.P.J., Walsh, E.J., Nolan, K.P., 2016b. Visualization of the vortex and reverse-flow structure of a separation bubble. J. Vis. 19, 175–177. doi:10.1007/s12650-015-0306-x.

Sunada, S., Sakaguchi, A., Kawachi, K., 1997. Airfoil Section Characteristics at a Low Reynolds Number. J. Fluids Eng. 119, 129. doi:10.1115/1.2819098.

Sunada, S., Yasuda, T., Yasuda, K., Kawachi, K., 2002. Comparison of wing characteristics at an ultralow Reynolds number. J. Aircr. 39, 331–338. doi:10.2514/2.2931.

Taira, K., Colonius, T., 2009. Three-dimensional flows around low-aspect-ratio flat-plate wings at low Reynolds numbers. J. Fluid

Mech. 623, 187–207. URL: http://www.journals.cambridge.org/abstract{_}S0022112008005314, doi:10.1017/S0022112008005314.

Tani, I., 1964. Low-Speed Flows Involving Bubble Separations. Prog. Aeronaut. Sci. 5, 70–103.

Videler, J.J., 2004. Leading-Edge Vortex Lifts Swifts. Science (80-.). 306, 1960–1962. URL: http://www.sciencemag.org/cgi/doi/10.1126/science.1104682, doi:10.1126/science.1104682.

Viola, I.M., Bartesaghi, S., Van Renterghem, T., Ponzini, R., 2013a. Delayed detached eddy simulation of sailing yacht sails, in: 3rd Int. Conf. Innov. High Perform. Sail. Yachts.

Viola, I.M., Bartesaghi, S., Van-Renterghem, T., Ponzini, R., 2014. Detached Eddy Simulation of a Sailing Yacht. Ocean Eng. 90, 93–103. doi:10.1016/j.oceaneng.2014.07.019.

Viola, I.M., Bot, P., Riotte, M., 2013b. Upwind sail aerodynamics: A RANS numerical investigation validated with wind tunnel pressure measurements. Int. J. Heat Fluid Flow 39, 90–101. URL: http://dx.doi.org/10.1016/j.ijheatfluidflow.2012.10.004, doi:10.1016/j.ijheatfluidflow.2012.10.004.

Viola, I.M., Flay, R.G.J., 2011a. Pressure distribution on sails investigated using three methods: on-water measurements, wind-tunnel measurements, and computational fluid dynamics, in: 20th Chesap. Sail. Yacht Symp.

Viola, I.M., Flay, R.G.J., 2011b. Sail aerodynamics: understanding pressure distributions on upwind sails. Exp. Therm. Fluid Sci. 35, 1497–1504. URL: http://linkinghub.elsevier.com/retrieve/pii/S0894177711001336, doi:10.1016/j.expthermflusci.2011.06.009.

Viola, I.M., Flay, R.G.J., 2011c. Sail pressures from full-scale, wind-tunnel and numerical investigations. Ocean Eng. 38, 1733–1743. URL: http://linkinghub.elsevier.com/retrieve/pii/S0029801811001764, doi:10.1016/j.oceaneng.2011.08.001.

Whidden, T., Levitt, M., 1990. The Art and Science of Sails: A Guide to Modern Materials, Construction, Aerodynamics, Upkeep, and Use. First ed., St Martins Pr.

White, F.M., 2011. Fluid Mechanics, 7th Edition. 7th ed., McGraw-Hill, New York, NY, USA. doi:10.1016/B978-0-12-546801-5.50017-7.

Widmann, A., Tropea, C., 2015. Parameters influencing vortex growth and detachment on unsteady aerodynamic profiles. J. Fluid Mech. 773, 432–459. doi:10.1017/jfm.2015.259.

Wong, J.G., Rival, D.E., 2015. Determining the relative stability of leading-edge vortices on nominally two-dimensional flapping profiles. J. Fluid Mech. 766, 611–625. doi:10.1017/jfm.2015.39.

Wu, J.C., 1981. Theory for Aerodynamic Force and Moment in Viscous Flows. doi:10.2514/3.50966.

Wu, J.Z., Ma, H.Y., Zhou, M.D., Wu J Ma H, Z.M., 2006. Vorticity and vortex dynamics. Springer. doi:10.1007/978-3-540-29028-5.

Ōtomo, S., Henne, S., Mulleners, K., Ramesh, K., Viola, I.M., 2021. Unsteady lift on a high-amplitude pitching aerofoil. Exp. Fluids 62, 1–18. URL: https://doi.org/10.1007/s00348-020-03095-2, doi:10.1007/s00348-020-03095-2.

Appendix

Consider a 2D plate at an angle of attack sufficiently large such that the flow is separated at both the leading and trailing edges, and the separated shear layers are oriented approximately in the streamwise direction (e.g. Fig. 6). Write two equations for the chord-normal velocity, which must be zero due to the Kutta condition, at both the leading and trailing edge. As we are only interested in an estimate of the sign of the bound circulation, the leading- and trailing-edge separated shear layers are represented with a single point vortex with circulation $-\Gamma$ and $+\Gamma$, respectively, at a streamwise distance δ_x from the plate edge.

The bound vortex is placed in the middle of the plate. At the leading edge, the sum of the chord-normal velocities due to the free stream velocity, the shear layer and the bound vorticity are

$$U \sin\alpha + \frac{\Gamma}{2\pi\delta_x}\cos\alpha - \frac{\Gamma_b}{\pi c} = 0. \tag{50}$$

At the trailing edge, the sum of the chord-normal velocities is

$$U \sin\alpha - \frac{\Gamma}{2\pi\delta_x}\cos\alpha + \frac{\Gamma_b}{\pi c} = 0. \tag{51}$$

Subtracting eq. 51 from eq. 50, gives

$$\frac{\Gamma}{\pi\delta_x}\cos\alpha - \frac{2\Gamma_b}{\pi c} = 0. \tag{52}$$

Solve for Γ_b to obtain

$$\Gamma_b = \frac{\cos\alpha}{2}\,\frac{c}{\delta_x}\,\Gamma\ > 0, \tag{53}$$

which is positive because every term on the right hand is defined positive.

CRediT authorship contribution statement

I.M. Viola: Conceptualisation, formal analysis and writing of the manuscript. **Abel Arredondo-Galeana:** Development of the complex potential and review of the manuscript. **Gabriele Pisetta:** Numerical simulations to test some of the hypothesis underlying this work and review of the manuscript.